Deep-Sea Research I 58 (2011) 338–349

Contents lists available at ScienceDirect

Deep-Sea Research I

journal homepage: www.elsevier.com/locate/dsri

Export and mesopelagic particle flux during a North Atlantic spring diatom bloom

Patrick Martin [a,*], Richard S. Lampitt [a], Mary Jane Perry [b], Richard Sanders [a], Craig Lee [c], Eric D'Asaro [c]

[a] National Oceanography Centre, European Way, Southampton, SO14 3ZH, UK
[b] School of Marine Sciences, University of Maine, USA
[c] Applied Physics Laboratory, University of Washington, USA

ARTICLE INFO

Article history:
Received 24 September 2010
Received in revised form
16 January 2011
Accepted 18 January 2011
Available online 28 January 2011

Keywords:
Neutrally buoyant sediment traps
Thorium-234
Particulate organic carbon flux
North Atlantic spring bloom
Transparent exopolymer particles

ABSTRACT

Spring diatom blooms are important for sequestering atmospheric CO_2 below the permanent thermocline in the form of particulate organic carbon (POC). We measured downward POC flux during a subpolar North Atlantic spring bloom at 100 m using thorium-234 (^{234}Th) disequilibria, and below 100 m using neutrally buoyant drifting sediment traps. The cruise followed a Lagrangian float, and a pronounced diatom bloom occurred in a 600 km^2 area around the float. Particle flux was low during the first three weeks of the bloom, between 10 and 30 mg POC m^{-2} d^{-1}. Then, nearly 20 days after the bloom had started, export as diagnosed from ^{234}Th rose to 360–620 mg POC m^{-2} d^{-1}, co-incident with silicate depletion in the surface mixed layer. Sediment traps at 600 and 750 m depth collected 160 and 150 mg POC m^{-2} d^{-1}, with a settled volume of particles of 1000–1500 mL m^{-2} d^{-1}. This implies that 25–43% of the 100 m POC export sank below 750 m. The sinking particles were ungrazed diatom aggregates that contained transparent exopolymer particles (TEP). We conclude that diatom blooms can lead to substantial particle export that is transferred efficiently through the mesopelagic. We also present an improved method of calibrating the Alcian Blue solution against Gum Xanthan for TEP measurements.

1. Introduction

Pronounced spring phytoplankton blooms with chlorophyll-*a* concentration ≥ 1.5 mg m^{-3} and primary productivity of 500–1500 mg C m^{-2} d^{-1} occur in the North Atlantic in response to spring stratification (Bury et al., 2001; Henson et al., 2009; Savidge et al., 1995). These blooms are initially dominated by diatoms, with a community-shift to smaller flagellates once diatoms have depleted surface silicate (Leblanc et al., 2009; Lochte et al., 1993; Sieracki et al., 1993). Such diatom blooms are known to trigger substantial export of fast-sinking phytodetrital aggregates that can carpet abyssal plains (Honjo and Manganini, 1993; Lampitt, 1985), and they are hence considered to be an important part of the biological carbon pump (Turner, 2002).

Although this broad outline (spring stratification→diatom bloom→silicon depletion+substantial particle export→community shift) is well established, we still lack a more detailed understanding of what triggers particle export, why such high particle export should occur, what the chemical and biological composition of the exported particles is, and how strongly the particle flux is attenuated in the mesopelagic, i.e. between 100 and 1000 m depth.

Aggregation of phytoplankton blooms appears to be driven by transparent exopolymer particles (TEP) (Alldredge and Jackson, 1995; Logan et al., 1995; Passow et al., 1994). These are a class of acidic polysaccharides excreted by diverse groups of phytoplankton, and even bacteria (Passow, 2002). They promote particle aggregation via their Stickiness and form the matrix of all marine snow particles studied to date (Alldredge et al., 1993; Dam and Drapeau, 1995; Engel, 2000; Passow and Alldredge, 1995b). TEP can thus be separate particles, or, by aggregating other particles such as phytoplankton cells, become a constituent of larger particles; it is in this latter sense that the term will mostly be used in this paper. Consequently, one might expect particle flux, or at least the flux of phytodetritus, to be strongly associated with TEP flux. For instance, a diatom bloom in a Norwegian fjord that failed to produce TEP did not aggregate (Kiørboe et al., 1996). However, high stickiness and aggregate formation did not lead to sedimentation of a diatom bloom in the Benguela upwelling (Kiørboe et al., 1998).

TEP have very rarely been measured in sediment traps. Reigstad and Wassmann (2007) found that TEP can be associated with peaks of *Phaeocystis* sp. export, but not always.

* Corresponding author. Tel.: +44 2380596336; fax: +44 238596247.
E-mail addresses: patrick.martin@noc.soton.ac.uk, pm@tellatale.eu (P. Martin).

0967-0637/$ - see front matter © 2011 Elsevier Ltd. All rights reserved.
doi:10.1016/j.dsr.2011.01.006

A two-year record of 500 m particle flux in the Santa Barbara Channel indicated that the sedimentation of diatoms was always associated with the presence of TEP in the sediment trap samples, but that only 67% of peaks in POC flux were associated with the peaks in TEP flux (Passow et al., 2001). While TEP therefore undoubtedly play a role in particle flux, sinking of some particle classes, perhaps faecal pellets, clearly does not depend upon TEP. In the case of a diatom bloom, however, one might expect that sedimentation should be driven by TEP-mediated aggregation.

The presence of biominerals has also been posited as an important factor in regulating particle flux, either by ballasting particles with excess density or by physically protecting organic matter from degradation (Armstrong et al., 2002; François et al., 2002; Ingalls et al., 2003; Klaas and Archer, 2002). Klaas and Archer (2002) concluded that $CaCO_3$ is a much more important ballast than opal, based on global relationships between mineral and organic carbon fluxes. François et al. (2002) concluded that particle export is also transferred more efficiently through the mesopelagic to depths >2000 m in $CaCO_3$-dominated regions than in opal- (i.e. diatom-) dominated regions. Based on changes in Si:C ratios with depth across different ocean basins, Ragueneau et al. (2006) concluded that diatom-dominated, more seasonal, regions remineralize a greater proportion of export flux in the mesopelagic, and suggested that organic matter in these areas might be more labile.

These conclusions are perhaps somewhat surprising, given that diatom blooms are thought to export a substantial fraction (up to 79%) of primary production (Buesseler, 1998), and result in aggregates that can sink apparently intact for thousands of metres (Lampitt, 1985). A recent re-analysis by Buesseler and Boyd (2009) concluded that a North Atlantic spring bloom was actually very efficient at exporting POC and transferring it through the mesopelagic.

Consequently, it is still unclear how efficiently POC flux is transferred to depth during a spring diatom bloom. However, there may be a question of timescale underlying these contradictory conclusions, as François et al. (2002) and Ragueneau et al. (2006) used annually averaged particle flux data, while Buesseler and Boyd (2009) used data gathered specifically during a bloom. Hence it is possible that particle flux during a spring bloom is transferred to depth more efficiently than at other times.

Measuring particle flux in the mesopelagic has proven difficult, as conventional (moored or surface-tethered) sediment traps are often unreliable at these depths, owing to hydrodynamic interferences and high zooplankton "swimmer" contamination (Buesseler et al., 2007). Neutrally buoyant sediment traps overcome these difficulties and should thus collect relatively unbiased samples (Buesseler et al., 2007).

We therefore estimated particle flux during a sub-polar North Atlantic spring bloom using neutrally buoyant sediment traps and ^{234}Th measurements.

2. Methods

A multi-disciplinary research cruise was undertaken in the Iceland Basin from 1 to 21 May 2008 aboard R/V *Knorr*. The cruise track followed a Lagrangian bio-optical float deployed in the surface mixed layer (but profiling to 250 m once daily). Four seagliders measured physical and bio-optical parameters in the area before, during, and after the cruise. Fig. 1 shows the study site, the trap and the ^{234}Th sampling locations, and indicates on a time-line the trap deployment periods and times of ^{234}Th sampling.

2.1. Neutrally buoyant sediment traps

Four deployments of 1–3 days each were undertaken with multiple neutrally buoyant sediment traps (PELAGRA; Lampitt et al., 2008) at depths between 150 and 750 m. Deployments are referred to as D1–D4 below. Each trap has four collection funnels (0.115 m^2 each) arranged around an ARGO float, leading to separate collection cups, and is equipped with an Idronaut CTD sensor recording every 30 s. The traps operated in isopycnal mode, i.e. following a surface of constant potential density rather than pressure. Collection cups were programmed to open 24 h after deployment (by sliding under the funnel), and to close again minutes before the trap ascended to the surface. During D1–D3, all cups on each trap collected simultaneously; during D4, the traps collected with two cups for the first 24 h, closed these, and collected with the remaining two cups for the next 24 h. Three collection cups per trap were filled with seawater from below 100 m to which were added 0.5% NaCl and 2% formaldehyde buffered with sodium tetraborate ($Na_2B_4O_7 \cdot 10\,H_2O$). One cup on each trap was filled with unpoisoned seawater. $SrCl_2$ was added to all poisoned cups on D2 prior to deployment to prevent dissolution of Acantharia, single-celled organisms with a shell of celestite (final Sr concentration of 88 mg L^{-1}; Beers and Stewart, 1970). $SrCl_2$ was not added on other deployments.

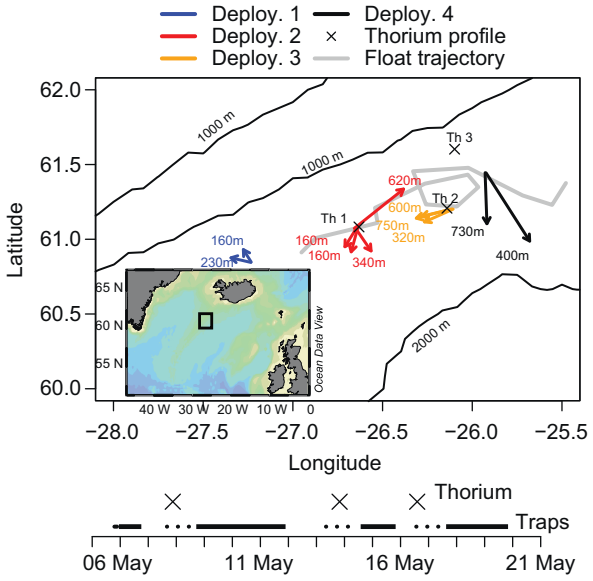

Fig. 1. Map of the study area. The inset shows the Iceland Basin, with the black box marking the region shown in the main map. The grey line shows the trajectory of the Lagrangian float from the day of the first sediment trap deployment until the end of the cruise. The trajectories of all sediment traps and the locations of the three ^{234}Th profiles are shown. The time-line at the bottom shows the deployment periods of the sediment traps (black bars) in relation to the times of ^{234}Th sampling (crosses). The solid part of each line shows the collection period for the traps (when collection cups were open), the dotted part shows the trap stabilisation period (when cups were still closed).

On recovery, 1 mL of 40% buffered formaldehyde was added to each poisoned cup, and the settled height of sediment in each sample was measured after 24 h. Samples from each trap were divided at sea with a Folsom splitter, and further on land with a rotary splitter. Fluxes of dry weight, POC, particulate organic nitrogen (PON), particulate inorganic carbon (PIC), celestite, biogenic silica (BSi), ^{234}Th and TEP were measured for each trap. Different cups on the same trap sometimes contained visibly different quantities of material, despite collecting simultaneously. In these cases, all poisoned samples of a trap were pooled before splitting. Owing to the difficulties of splitting the resulting large volumes with a Folsom splitter, cups were treated individually in those cases in which material was evenly distributed between cups. Swimmers were removed under a Wild dissecting microscope (60x–120x magnification) from all samples except from the sub-samples for ^{234}Th.

A trap deployment was deemed successful if the trap remained at a particular depth, as measured by the Idronaut CTD, during the period of sample collection. The trap trajectories while underwater were estimated as a straight line between deployment and surfacing positions.

2.2. POC/PON and dry weight

Sub-samples between 2 and 15 mg dry weight were filtered onto pre-combusted (550 °C, 4 h), pre-weighed Whatman GF/F filters, rinsed with 18.2 MΩ cm^{-1} (MilliQ) water, dried at 40 °C for 24 h, and weighed. They were then fumed with concentrated HCl in a desiccator for 24 h, dried again at 40 °C for 24 h, wrapped in pre-combusted (550 °C, 4 h) aluminium discs (Elemental Microanalysis, UK), and pelleted. C and N were analysed on a Flash 1112 Elemental Analyser (Thermo Finnigan). Samples were analysed in triplicate for D2 and D3 traps, with relative standard deviations (RSD) of $<9.5\%$, and mostly $<6\%$ for dry weight, and $<8\%$ and $<12\%$ for POC and PON, respectively. For D1 and D4, the mean RSD of the other samples was applied (5% dry weight; 5% POC; 7% PON).

2.3. PIC, celestite, and BSi

Sub-samples identical to those analysed for POC were filtered onto 0.4 μm Millipore polycarbonate filters, rinsed with MilliQ water, and stored at −20 °C until analysis. Filters for PIC and celestite were digested in 1 mol L^{-1} acetic acid for 24 h, and dissolved Ca, Sr, and Na were analysed on a PerkinElmer Optima 4300DV inductively coupled plasma optical emission spectrometer with a PerkinElmer AS93 Plus autosampler, concentric glass nebuliser, and a baffled, cyclonic spray chamber. PIC was calculated assuming that all PIC was $CaCO_3$, and celestite was calculated assuming all Sr was $SrSO_4$ (celestite is the only known marine biomineral containing Sr as a major constituent). The low Na concentrations in the digests showed that sea-salt had been fully removed by the MilliQ rinse.

Filters for BSi were digested in 0.2 mol L^{-1} NaOH at 90 °C for 3 h, the solution neutralised with HCl, and then analysed on a SEAL QuAAtro autoanalyser. Opal was calculated assuming 10% water content (Mortlock and Froelich, 1989; Salter et al., 2007). Analyses were duplicated (i.e. two sub-samples analysed) whenever enough material was available; percentage difference between duplicates was $<30\%$ (and mostly $<10\%$) for opal, $<23\%$ for PIC, and $<23\%$ for celestite (except for D2#160, which had low Sr flux with a percentage difference of 89%).

2.4. Transparent exopolymer particles (TEP)

TEP were measured using a dye-binding assay described by Passow and Alldredge (1995a). Filtered particles were stained with a 0.02% Alcian Blue solution (Sigma Aldrich, UK), dissolved in 80% H_2SO_4, and the absorbance of the acid measured on a Hitachi U-2800 spectrophotometer. The absorbance was then converted to units of grams of Gum Xanthan equivalents (GX eq.) using a calibration curve.

The calibration curve was established by filtering and staining a range of aliquots (0.5–6 mL) of a $<0.1\%$ solution of Gum Xanthan (Sigma Aldrich, UK). The original protocol specifies that one set of Gum Xanthan filters is stained, digested in H_2SO_4, and the absorbance measured, while a second set of filters is prepared to measure only Gum Xanthan dry weight (hence left unstained). However, the variability in dry weight and absorbance at each volume was high during initial trials, and hence we changed the protocol to measure both absorbance and dry weight on the same filter.

0.5–6 mL aliquots of Gum Xanthan solution (3 replicates per volume) were filtered onto pre-weighed polycarbonate filters, stained, rinsed, and dried at 60 °C for 24 h. Filters were weighed, soaked in 80% H_2SO_4, and the absorbance measured. The filter dry weights must then be corrected for the mass of Alcian Blue: 10–200 μL aliquots of dye solution (for which the mass of Alcian Blue can be calculated from the concentration) were mixed with 80% H_2SO_4 and the absorbance measured after 2 h. The relationship between absorbance and mass of Alcian Blue (Supplementary Fig. 1) was used to correct the dry weight of each stained filter. This correction was critical, as the calculated weight of Alcian Blue contributed 20–60% of the change in filter weight after filtering and staining the Gum Xanthan. Alcian Blue powder for the dye solution was weighed out on a Sartorius microbalance to achieve a concentration of exactly 0.02% to allow an accurate correction. Moreover, three separate experiments showed that the absorbance of a given quantity of Alcian Blue is not affected by drying at 60 °C (Supplementary Fig. 2).

The calibration curve used to calculate mass GX eq. from sample absorbance was linear over a range of absorbances exceeding the sample absorbances with $R^2=0.97$ (Fig. 2). While it is usually appropriate to calculate a calibration curve only over the range of values observed in the samples, we have used the curve as calculated over the full range of values in Fig. 2. The data at absorbances <0.2 were more scattered, and using the full range of values yielded a more accurate curve (see below). If the upper range of the calibration data had been excluded, the weight of the unusually low data point at 15 μg Gum Xanthan would also have been increased.

TEP were then measured in the samples using aliquots between 1/1600 and 1/370 of the original sample. For each sample, two dilutions were prepared with a NaCl solution (35 g NaCl in 1 L MilliQ), and 1 mL was filtered in triplicate at each dilution, and stained, etc., as above. For D1 samples, aliquots of the concentrated sample solution were filtered as well. For each dilution, the mean absorbance of the triplicate measurements was used to calculate the TEP concentration per mL of the stock solution, and the sample TEP content was calculated from the mean of the two dilutions. Percentage differences in TEP content

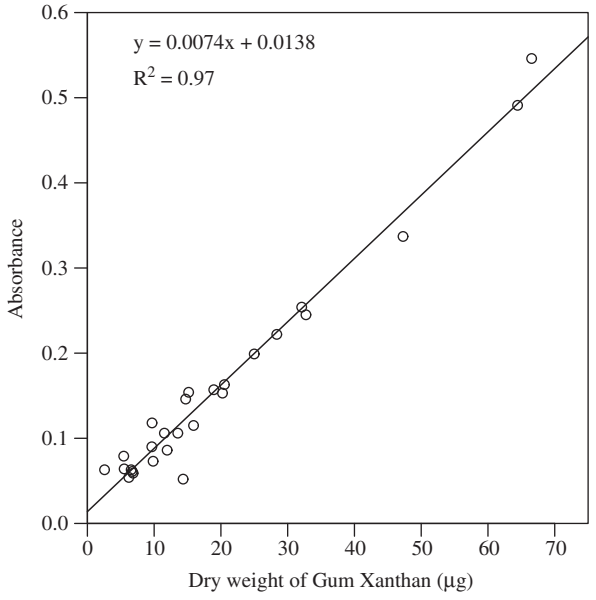

Fig. 2. Calibration curve for TEP to convert measured sample absorbances to units of μg Gum Xanthan equivalents.

between the two dilutions were 10–22%, except for D3#750, where the difference was 34%. Applying a restricted calibration curve, using only data with absorbance <0.2, increased the percentage difference between the two dilutions, suggesting that the curve using the full range of data was more accurate. Absorption from unstained particles was negligible.

2.5. ^{234}Th measurements

^{234}Th has a half-life of 24.1 days and its radioactive disequilibrium from its parent, uranium-238, is indicative of particle transport occurring over the previous days to weeks (Buesseler et al., 1992; Murray et al., 1996). Daily ^{234}Th export can be estimated from a single profile using a steady-state (SS) model, which calculates the quantity of ^{234}Th that must be exported daily to maintain the observed depletion, assuming that the ^{234}Th concentration does not change over time. Alternatively, if multiple profiles are measured, a non-steady-state (NSS) model can be used, which accounts for temporal changes in the depletion (Savoye et al., 2006). Both models were used in this study, and the NSS model was calculated according to Buesseler et al. (1992): the downward ^{234}Th flux is calculated separately for each sampled depth layer from the change in ^{234}Th concentration over time, in-growth from ^{238}U, decay of ^{234}Th, and ^{234}Th flux into the layer from the layer above. POC flux was calculated from ^{234}Th flux using POC:^{234}Th ratios measured on sinking particles caught with the PELAGRA traps. The greatest uncertainties with this method are whether a steady-state assumption is justified, and how well POC:^{234}Th concentrations can be constrained.

Total water column ^{234}Th was measured using a 10 L MnO_2 co-precipitation technique (Rutgers van der Loeff and Moore, 1999; Thomalla et al., 2006). Water was collected with Niskin bottles at ten depths between 5 and 400 m at three stations (the first two directly adjacent to the Lagrangian float), and amended with 3 drops of concentrated ammonia solution, 125 μL of concentrated $KMnO_4$ solution, and 50 μL of concentrated $MnCl_2$ solution. Samples were filtered after 8 h through 142 mm diameter polycarbonate filters (0.8 μm), rinsed with MilliQ water, allowed to dry, and folded reproducibly into 18×18 mm^2 parcels. Extraction efficiency was assessed by double-precipitation of nine samples, and found to be 100 ± 3%. Counting efficiency was measured using five samples from 1000 m, where ^{234}Th is in secular equilibrium with ^{238}U.

^{234}Th in sinking particles was measured in sub-samples from PELAGRA Deployments 1–3, filtered and folded as for water column ^{234}Th measurements (samples from Deployment 4 could not be processed for ^{234}Th before the cruise ended). POC:^{234}Th ratios were calculated from POC and ^{234}Th fluxes measured in the traps. ^{234}Th in all samples was measured with a Risø National Laboratory GM-25-5A low-level β-counter in anti-coincidence mode. Samples were counted on board and throughout the following six months to ensure that activity decreased according to the half-life of ^{234}Th. The activity of ^{238}U was calculated from salinity (Chen et al., 1986).

2.6. Chlorophyll and silicate

Chlorophyll was measured by a fluorometer on the Lagrangian float (WetLabs FLNTU, excitation wavelength 470 nm). This sensor was calibrated against a similar fluorometer on the CTD rosette. Chlorophyll was analysed from water samples concurrently collected by the CTD rosette; samples were filtered onto GF/F filters, extracted with 90% acetone for 24 h in the dark at -20 °C, and measured on a Turner Designs AU-10 fluorometer. The relationship between measured chlorophyll concentration from the bottle samples and the fluorescence measured *in situ* by the rosette-mounted fluorometer was then applied to the fluorescence measured by the float. The relative standard deviation of the chlorophyll concentration thus calculated from the float was 30–40% (E. D'Asaro, pers. comm.).

Samples for silicate were taken throughout the cruise, and frozen at sea (-20 °C). Silicate was then measured after transporting back to land on a Lachat Quickchem 8000 Flow Injection Analysis System using standard absorptiometric techniques. Samples were slowly thawed in the dark at room temperature for 24 h and vigorously vortexed before analysis (Gordon et al., 1994). The data presented here are the mean concentration in the upper 20 m ($n=2$–3 samples), and stations thought to have been outside of the bloom patch (see Section 3.1) are omitted here.

2.7. Satellite imagery

Daily composite images were created by averaging individual MODIS and MERIS images on a pixel-wide basis and gridding them on a 1 km resolution grid.

3. Results

3.1. Surface biogeochemical and hydrographical setting

The bloom did not occur homogeneously over a large area. The Lagrangian float followed a distinct patch of enhanced chlorophyll concentration that was dominated by diatoms. This patch was clearly visible in MODIS/MERIS sea-surface colour images (Fig. 3), and could be distinguished from the surrounding waters with the bio-optical measurements taken by the gliders and from the ship (A. Gray, pers. comm.). The patch was 600 km^2 on 6 May (Fig. 3a), but had shrunk to 250 km^2 by 11 May (Fig. 3b). This patch was intensively studied during the cruise, and constituted the bloom that we discuss in this paper.

Chlorophyll fluorescence and dissolved oxygen as measured by the seagliders increased from 19 April, indicating that the bloom started approximately 10 days prior to the cruise. Nutrient concentrations in the surface mixed layer decreased due to phytoplankton production: nitrate declined from 11 to 8.5 μM over the course of the cruise, while silicate decreased from 4 to ≤1 μM over the same period, and was <2 μM by 7 May. Consequently, there was a phytoplankton community shift from diatom dominance to picoeukaryotes, with shipboard observations suggesting a peak in diatom abundance between 8 and 11 May (M. Sieracki, pers. comm.). Chlorophyll as measured by the float rose from close to 1 mg m^{-3} to a peak of nearly 4 mg m^{-3} between 1 and 12 May, and declined thereafter to around 1 mg m^{-3} again. By the time of the final trap deployment (17 May), chlorophyll and diatom numbers in the patch had decreased substantially, making it harder to track the patch.

3.2. Trap deployments

Traps were successfully deployed eleven times during four separate deployments, which are referred to as Deployment Number#Depth (e.g. D3#750 refers to the 750 m trap on the third deployment). Deployment depths and durations are listed in Table 1, and profiles of trap depth against time for each trap are shown in Supplementary Fig. 3. Trap trajectories are shown in Fig. 1.

3.3. Trap-derived particle flux

Fluxes of total dry weight, POC, PON, PIC, BSi, celestite, ^{234}Th, and TEP for each trap are summarised in Table 2.

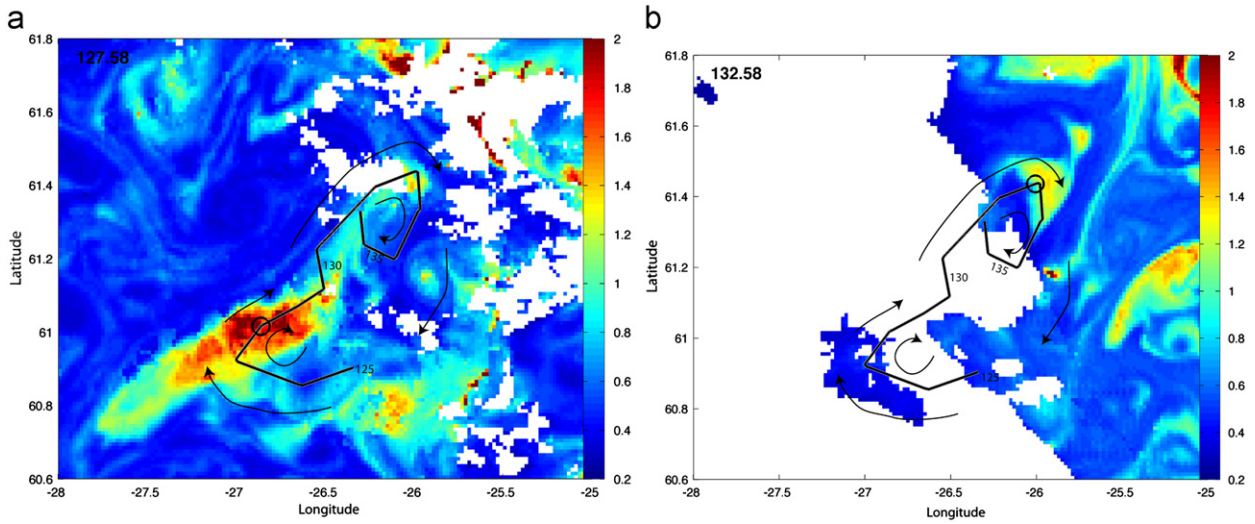

Fig. 3. MODIS/MERIS daily composite chlorophyll-*a* images of the extent of the float patch on (a) 6 May and (b) 11 May. Scale bars show chlorophyll concentration in mg m^{-3}. The track of the Lagrangian float between 4 May and 19 May is marked with the black line. The circle in each image indicates the float position at the time of the image, and numbers along the float trajectory mark the float position on the corresponding year–day number (125=4 May, 130=9 May, 135=14 May). The arrows show the approximate direction of the surface currents (A. Gray, pers. comm.) (For interpretation of the references to colour in this figure, the reader is referred to the web version of this article.)

Table 1
Summary of trap deployments. Note that all traps were deployed 18–24 h before cups opened. In the case of D4, only one trap was deployed at each depth, but they collected in time-series mode: two collection cups were open for the first 24 h, closed, and then the next two cups opened.

Trap ID (Deployment number#Depth)	Date/time of cup opening	Date/time of cup closing
D1#140	5/5/08 23:10	6/5/08 15:10
D1#230	6/5/08 00:55	6/5/08 15:55
D2#160[a]	8/5/08 19:25	11/5/08 19:25
D2#340	9/5/08 18:55	11/5/08 18:55
D2#160[a]	8/5/08 19:10	11/5/08 19:10
D2#620	9/5/08 06:40	11/5/08 18:40
D3#320	14/5/08 17:40	15/5/08 17:40
D3#600	14/5/08 15:55	15/5/08 15:55
D3#750	14/5/08 16:10	15/5/08 16:10
D4#400[b]	17/5/08 17:50	18/5/08 17:50
D4#400[c]	18/5/08 17:55	19/5/08 17:55
D4#730[b]	17/5/08 17:05	18/5/08 17:05
D4#730[c]	18/5/08 17:10	19/5/08 17:10

[a] Two traps were deployed at the same depth.
[b] First 24 h of collection.
[c] Second 24 h of collection.

3.3.1. *POC flux and POC:PON ratios*

Fig. 4a–d shows POC fluxes and POC:PON ratios for each deployment. POC flux was very low during the first two deployments (10–30 mg POC m^{-2} d^{-1}), but then increased to 75–165 mg POC m^{-2} d^{-1} during the final two deployments, peaking during D3. During D2 and D3, fluxes caught by the shallowest traps were two- to three-fold lower than those caught by the deeper traps, which we attribute to temporal and spatial variability in particle flux.

Molar POC:PON ratios ranged from 4.4 to 6.7, with higher values in the D3 and D4 traps, and a mean weighted by POC flux of 6.1. The correlation between POC:PON and depth was not significant (Spearman's rank correlation, $rho=0.452$, $p=0.121$, $n=13$).

POC contributed 8–13% of total mass flux in all cups (Table 2), with the highest percentages during D1 and D2, and in D4#400. The D3 traps contained substantial quantities of diatom-opal, and these samples contained the lowest percentage POC contribution.

Fig. 5 shows photographs of the D3 samples (24 h collection). The collection cups are 500 mL Nalgene jars, and the settled volume flux was 1000–1500 mL m^{-2} d^{-1}. The photos clearly show that the settling material was predominantly phytodetrital, although some faecal pellets were also present.

3.3.2. *Opal flux and Si:POC ratios*

Opal flux (as hydrated SiO_2) ranged from about 25 to 1000 mg m^{-2} d^{-1}. Traps during D1 and D2 caught the lowest, and D3#600 and D3#750 the highest opal fluxes. During D4, opal fluxes were around half those during D3. The percentage contribution by opal to total dry weight was 15–25% during D1 and D2, and 40–60% in D3 and D4 (Fig. 4e–h).

The molar Si:POC ratios ranged from 0.2 to 1.3, and showed a significant increase with depth (Fig. 4e–h, Spearman's rank correlation, $rho=0.651$, $p=0.016$, $n=13$). However, this trend is also a function of time, as the deeper traps with high Si:POC were deployed during D3 and D4 (see Section 4.4).

3.3.3. *PIC and celestite flux*

PIC flux was very low throughout the cruise (0.14–18 mg m^{-2} d^{-1}), and hence the rain ratio (PIC:POC) never rose above 0.13. As for most components, PIC flux also increased from D1/D2 to D3/D4. The percentage of total mass flux contributed by $CaCO_3$ (as calculated from Ca flux) was notably variable; the two D1 traps differed by a factor of 10 in this measure, and the D2 traps differed by a factor of 1.5, even between the two 160 m traps.

PIC variability was similar to that of celestite, which was detected in all traps on D2 and D4: the percentage contribution of celestite to total mass flux varied by a factor of 10 on D2, and by a factor of 2 on D4. Celestite contributed up to 10% of total mass flux during D2 and D4 (up to 100 mg celestite m^{-2} d^{-1}). Celestite is precipitated exclusively by Acantharia, single-celled organisms related to the Radiolaria. Although surface-dwelling as adults, Acantharia can form rapidly sinking reproductive cysts. We found cysts of the type reported by Martin et al. (2010) in samples from all traps upon recovery; hence the lack of measurable particulate celestite in D1 and D3 must be due to dissolution of this very soluble biomineral (Beers and Stewart, 1970).

Table 2
Summary of fluxes of chemical phases into the PELAGRA sediment traps, and elemental ratios. Note that for biominerals, the fluxes are as mass of mineral, not element, e.g. "opal flux" is the flux of hydrated SiO_2, not of Si.

Trap	Dry weight flux ($mg\,m^{-2}\,d^{-1}$)	POC flux ($mg\,m^{-2}\,d^{-1}$)	PON flux ($mg\,m^{-2}\,d^{-1}$)	POC:PON molar ratio	Opal flux ($mg\,m^{-2}\,d^{-1}$)	Si:POC molar ratio	PIC flux ($mg\,m^{-2}\,d^{-1}$)	Celestite flux ($mg\,m^{-2}\,d^{-1}$)	TEP flux ($mg\,GX\,eq.\,m^{-2}\,d^{-1}$)	TEP:POC ratio ($mg\,GX\,eq.\,mg^{-1}$)	^{234}Th flux ($dpm\,m^{-2}\,d^{-1}$)
D1#140	121.0	15.4 ± 0.8	3.1 ± 0.49	5.80 ± 0.96	28 ± 0.84	0.33 ± 0.020	0.14 ± 0.02	ND	ND	NA	141.23
D1#230	138.0	14.4 ± 0.7	3.1 ± 0.52	5.42 ± 0.95	34 ± 3.7	0.43 ± 0.052	1.8 ± 0.27	ND	ND	NA	182.60
D2#160	94.3	10.2 ± 0.3	2.7 ± 0.25	4.41 ± 0.43	24 ± 5.0	0.43 ± 0.092	1.2 ± 0.14	1.4 ± 1.2	ND	NA	243.67
D2#340	240.2	30.6 ± 1.7	6.7 ± 0.32	5.33 ± 0.39	63 ± 3.8	0.37 ± 0.030	3.3 ± 0.5	26.2 ± 2.9	ND	NA	605.71
D2#160	119.0	13.3 ± 0.7	3.0 ± 0.34	5.17 ± 0.65	31 ± 1.9	0.43 ± 0.034	1.0 ± 0.22	11.1 ± 2.4	ND	NA	249.39
D2#620	235.0	27.2 ± 1.8	6.3 ± 0.68	5.04 ± 0.64	32 ± 1.3	0.21 ± 0.017	1.9 ± 0.36	18.2 ± 1.3	ND	NA	311.47
D3#320	878.4	76.2 ± 6.1	17.4 ± 2.20	5.11 ± 0.76	398 ± 39.8	0.95 ± 0.121	6.2 ± 0.81	ND	30	0.39	2200.65
D3#600	1874.6	164 ± 4.1	29.1 ± 2.46	6.59 ± 0.58	1040 ± 83.2	1.15 ± 0.096	17.8 ± 2.49	ND	122	0.74	5476.98
D3#750	1933.0	154 ± 4.8	30.4 ± 3.90	5.91 ± 0.78	1089 ± 315.8	1.28 ± 0.374	15.3 ± 1.84	ND	118	0.77	6014.65
D4#400[a]	1047.7	120 ± 5.8	21.5 ± 1.48	6.54 ± 0.55	432 ± 47.5	0.65 ± 0.078	13.0 ± 1.95	101.5 ± 13.2	42	0.35	NM
D4#400[b]	929.4	112 ± 5.4	19.5 ± 1.36	6.69 ± 0.57	498 ± 54.8	0.81 ± 0.097	13.3 ± 2.00	80.7 ± 10.5	37	0.33	NM
D4#730[a]	994.8	95.2 ± 4.6	17.6 ± 1.24	6.31 ± 0.54	605 ± 66.6	1.15 ± 0.139	9.3 ± 1.40	46.3 ± 6.0	35	0.37	NM
D4#730[b]	779.1	75.1 ± 3.7	13.7 ± 1.01	6.40 ± 0.57	436 ± 48.0	1.05 ± 0.127	9.0 ± 1.35	58.0 ± 7.5	47	0.63	NM

ND = not detected; NA = not applicable; NM = not measured.
[a] First 24 h of collection.
[b] Second 24 h of collection.

Dissolution was prevented in D2 with $SrCl_2$ addition, and in D4 the flux of acantharian cysts was probably so high that the preservative solution saturated from just a proportion of the cysts dissolving (Martin et al., 2010). Therefore, except for D2, the estimates of celestite flux are significant underestimates, and some celestite was certainly present in D1 and D3.

3.3.4. TEP flux

TEP were barely detectable in D1 and D2, but reached 30–120 mg GX eq. $m^{-2}\,d^{-1}$ during D3 and D4. Although absorbances of stained filters from D1 and D2 were always slightly higher than blanks, the small positive *y*-intercept of the calibration line (Fig. 2) brought the calibrated TEP concentration in these samples to zero. This indicates that a small quantity of TEP was present, but not enough to be quantified using our calibration. TEP fluxes were highest in D3#600 and D3#750, which also had the highest TEP:POC ratios (0.8 and 0.7 mg GX eq. mg^{-1}). TEP flux in D3#320 and in the D4 traps was < 50 mg GX eq. $m^{-2}\,d^{-1}$, and TEP:POC in these samples was < 0.4 mg mg^{-1} (apart from D4#730 on Day 2, in which TEP:POC was 0.6 mg mg^{-1}).

These results should be treated with some caution, given the scatter around the calibration curve at the low absorbances measured in our samples. However, initial trial measurements while developing the method gave very similar absorbances, although a good calibration had not yet been established. Moreover, this assay actually measures not the absolute amount of TEP, but the amount of binding sites available for the dye. Our data are only quantitatively comparable to other studies if the number of binding sites per amount of TEP is constant, but this could vary depending on factors such as the species producing the TEP and the extent of degradation (U. Passow, pers. comm.). Consequently, we consider our TEP data to be semi-quantitative, clearly demonstrating the presence of TEP in the D3 and D4 samples, and indicating the presence of a small amount of TEP in the D1 and D2 samples.

3.3.5. ^{234}Th flux from traps and POC:^{234}Th ratios

^{234}Th fluxes ranged from 140 to 600 dpm $m^{-2}\,d^{-1}$ during D1 and D2, with POC:^{234}Th ratios of 3.5–9.1 dpm $m^{-2}\,d^{-1}$ (Fig. 4i–k). There was no clear trend with depth, although the highest ^{234}Th fluxes were found in the deeper traps. ^{234}Th flux was substantially higher in the D3 traps, with 2200, 5500, and 6000 dpm $m^{-2}\,d^{-1}$ in D3#320, D3#600, and D3#750, respectively. POC:^{234}Th ratios in these traps were 2.9, 2.5, and 2.1, respectively. Overall, there was no clear trend in POC:^{234}Th ratios with depth, but it appears as though the ratio was decreasing over time (Fig. 4i–k).

3.4. Water column ^{234}Th deficits and diagnosed ^{234}Th fluxes

The three profiles of total ^{234}Th activity are shown in Fig. 6, with the integrated (to 100 m) deficit of ^{234}Th for each profile, calculated by trapezoid integration, in Fig. 7. Locations of the profiles are marked in Fig. 1. The small deficit in Profile 1 (9400 ± 4700 dpm m^{-2}, Fig. 7) shows that export was low in the weeks before 7 May. The deficit of Profile 2 was much greater ($47{,}000 \pm 5200$ dpm m^{-2}, Fig. 7), indicating that substantial export occurred between 7 and 12 May. Profile 3 shows a smaller deficit, owing to the shallower ^{234}Th depletion (Fig. 6). However, Profile 3 was taken approximately 10 km north of the Lagrangian float and outside of the bloom patch. Consequently, we make use of only Profiles 1 and 2 to calculate ^{234}Th fluxes.

An SS model applied to the first profile yielded a flux at 100 m of 240 ± 430 dpm $m^{-2}\,d^{-1}$, which we take as a level of flux representative of the previous weeks. An NSS calculation between the first and second profile (6 days apart) yields a ^{234}Th flux of

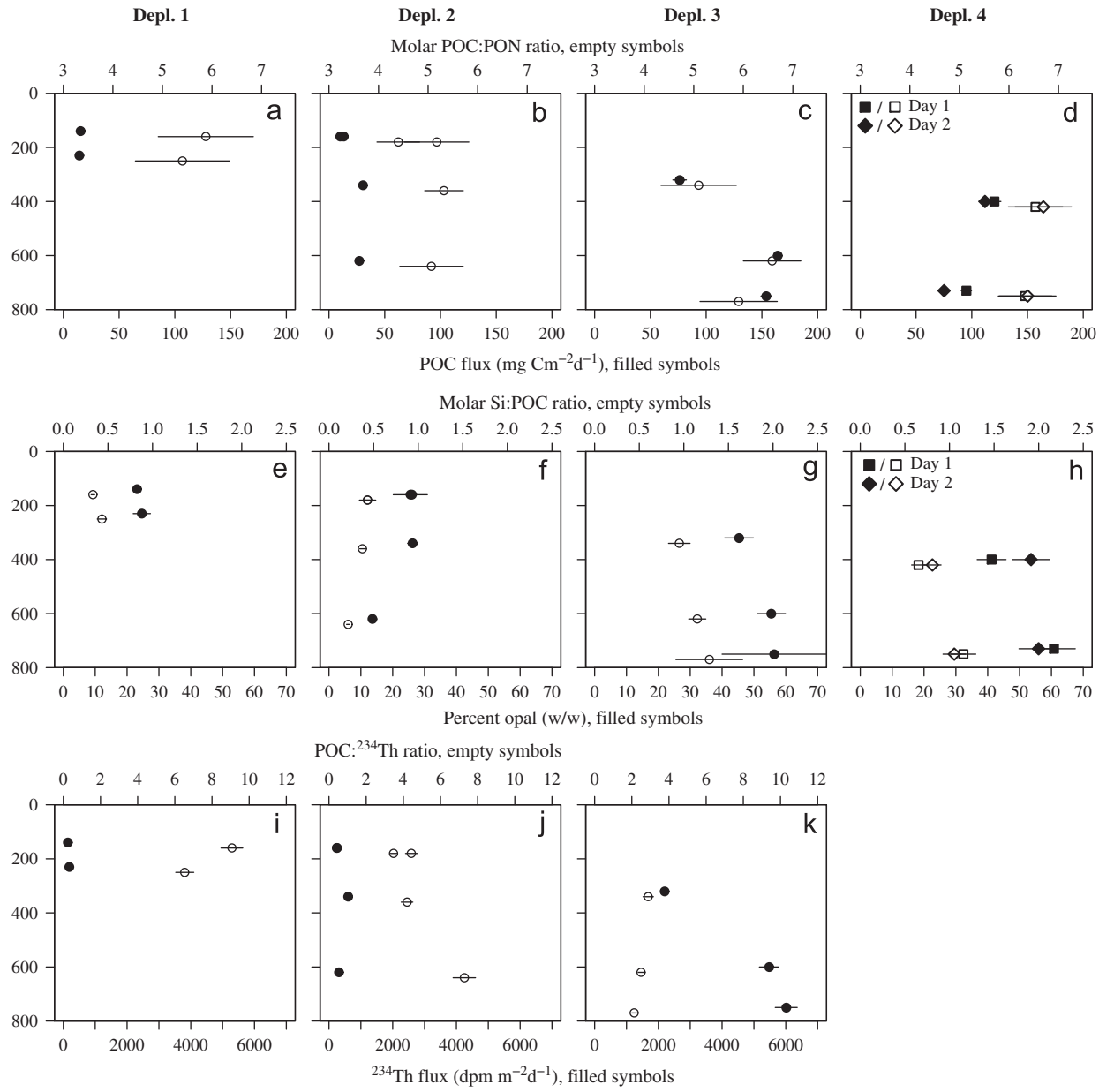

Fig. 4. (a–d) POC fluxes and molar POC:PON ratios for each sediment trap. Symbols for POC:PON ratios have been offset by 20 m from symbols for POC flux to prevent error bars from overlapping. (e–h) Percentage contribution by opal to total dry weight, and molar Si:POC ratios, for each sediment trap. Symbols for Si:POC ratios have been offset by 20 m from symbols for percentage opal content to prevent error bars from overlapping. (i–k) ^{234}Th fluxes and POC:^{234}Th ratios for each sediment trap (note that no ^{234}Th measurements were taken from D4 traps due to time constraints). All error bars are one standard deviation, showing the analytical error of the measurement based on propagated uncertainties.

7400 ± 2400 dpm m^{-2} d^{-1} during this period. The importance of using an NSS model in this case is illustrated by the fact that an SS model applied to the second profile would yield a flux of only 1350 ± 400 dpm m^{-2} d^{-1}, or 20% of the NSS flux.

4. Discussion

The ^{234}Th- and trap-derived particle flux estimates, and the time-series of chlorophyll and silicate, are summarised and plotted on a common *x*-axis in Fig. 8. This plot also shows the local chlorophyll and silicate concentrations (mean of upper 20 m) measured from the CTD cast closest to each trap deployment and ^{234}Th profile. These measurements matched the overall trends in chlorophyll and silicate at each time-point well, suggesting that spatial variability within the patch was much smaller than temporal variability.

4.1. Timing of bloom sedimentation

The ^{234}Th profiles clearly show that a large export event occurred between 7 and 12 May, around 20 days after the bloom had started. This is supported by spikes appearing below the mixed layer in the chlorophyll and backscatter sensors on the gliders and the CTD rosette between 5 and 8 May, indicating that aggregates were sinking (Briggs et al., in prep.). By this time, silicate concentrations were low ($\sim$1 μM) and did not decrease very much further (Fig. 8). Diatom growth during North Atlantic spring blooms is thought to be terminated by silicate limitation

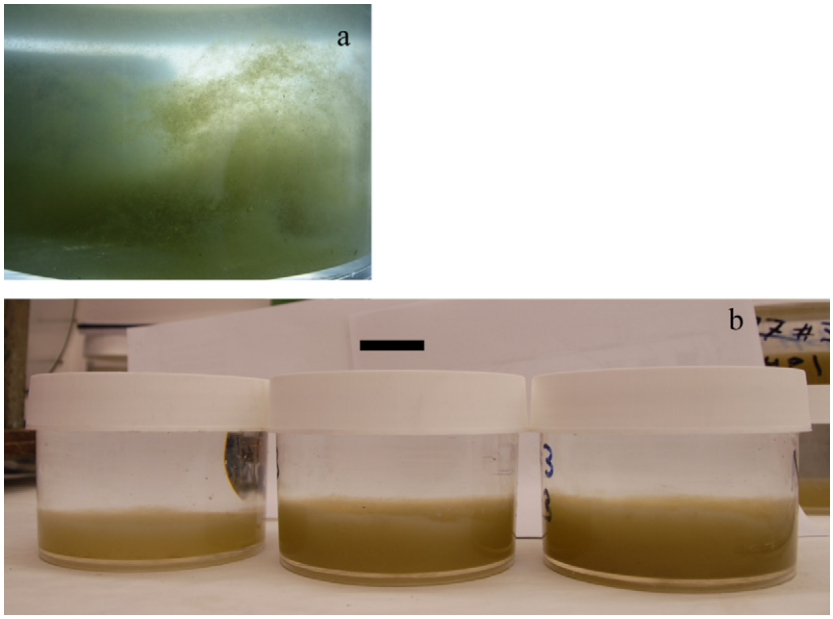

Fig. 5. Photographs of sediment trap samples from the third deployment. (a) Close-up photo of a sample from D3#750, showing the loose, fragile, nature of the trapped particles; (b) one sample each from (left to right) D3#320, D3#600, and D3#750, as photographed on board. Scale bar=2.5 cm.

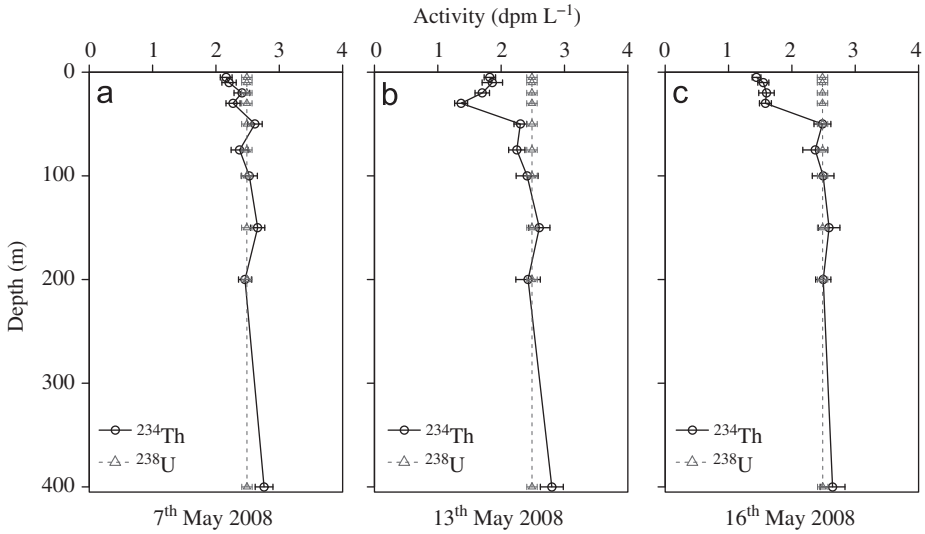

Fig. 6. Vertical profiles of ^{234}Th and ^{238}U activity concentration. Error bars are one standard deviation, showing the analytical uncertainty based on propagated errors. The first two profiles were taken directly adjacent to the Lagrangian float, i.e. within the float patch, but the third profile was taken outside of the patch.

(Henson et al., 2006; Leblanc et al., 2009; Savidge et al., 1995; Sieracki et al., 1993), and that clearly occurred during the present study as well.

Surprisingly, the D2 traps, which collected between 8 and 11 May, did not catch this export pulse. However, all but the deepest trap on D2 drifted southward and perpendicular to the float. Given the sharply delimited southern boundary of the patch, which drifted north-eastwards (Fig. 3a), it is possible that the D2 traps collected particles mostly from outside of the patch—with the exception of the 620 m trap that was probably too deep to catch the export event yet.

The D3 traps, however, caught a large pulse of opal- and TEP-rich particles that very probably were derived from this export event, suggesting that the exported material reached 750 m depth between 14 and 15 May. If export below 100 m started on 8 May, that would imply a minimum sinking rate of 110 m d^{-1}, which is within the range of sinking speeds reported for phytodetritus and marine snow (50–200 m d^{-1}; Turner, 2002), and slightly higher than the range of 65–90 m d^{-1} calculated by Briggs et al. (in prep.) during the cruise from the spikes in seaglider optical backscattering.

Why the shallower trap, D3#320, caught less material than the two deep D3 traps is unclear. It is possible that the traps lagged behind the patch, which drifted north-westward, and thus collected partly below adjacent, low-chlorophyll water. In such a case, deeper traps might still collect particles derived only from within the patch for several more days, while shallower traps will start to catch more recent particles from the overlying water, and thus contain less material (and sediment traps do not necessarily collect particles from directly above; see Siegel et al., 2008). Alternatively, particle export might have decreased after 12 May. The shallower trap would then also have caught less material than the deeper traps. We cannot resolve this question,

but it seems likely that the flux caught in D3#320 was less representative of flux during the height of the export event than the flux caught in the two deep D3 traps.

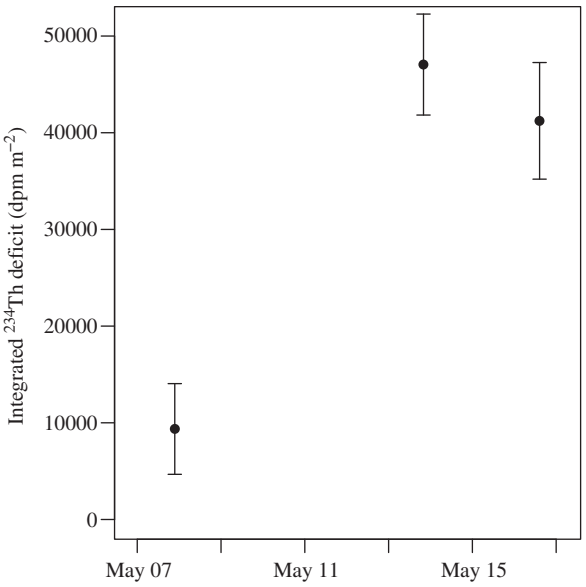

Fig. 7. Calculated deficit of ^{234}Th against time from each of the three profiles. The deficits were calculated by trapezoidal integration to 100 m. The strong increase in the deficit between the first two profiles indicates that substantial particle export occurred in the intervening period.

4.2. Magnitude of 100 m POC export

Converting the daily ^{234}Th export at 100 m into POC export is complicated in this case by the uncertainty in the most appropriate POC:^{234}Th ratio to use: we were unable to sample material from the large flux event as it left the surface, and POC:^{234}Th ratios invariably decrease with depth (Buesseler et al., 2006; Maiti et al., 2010). Therefore, the POC:^{234}Th ratios measured in D3#600 and D3#750 are almost certainly lower than the ratio at 100 m. However, it appears as though the POC:^{234}Th ratio was decreasing over the course of the cruise (Fig. 4i–k), suggesting that the POC:^{234}Th ratio at 100 m for the high flux event was lower than in D1 (9.1 μmol POC dpm^{-1}). This is consistent with the greater TEP-richness of the D3 and D4 material, as Th has a high affinity for acidic polysaccharides and TEP-rich material should hence have lower POC:^{234}Th ratios (Passow et al., 2006).

Given this substantial uncertainty, we present the 100 m POC export between 7 and 13 May as a function of the POC:^{234}Th ratio (Fig. 9). Realistically, the appropriate POC:^{234}Th ratio was probably between 4 and 7 μmol dpm^{-1} (globally, POC:^{234}Th ratios tend to fall within this range as well; Buesseler et al., 2006), which translates to a POC export between 360 ± 120 and 620 ± 200 mg POC m^{-2} d^{-1} at 100 m. This export estimate spans the range of values reported by Buesseler et al. (1992) for a North Atlantic bloom at 48°N. It also agrees both with a model of the 2008 sub-polar spring bloom, which yields POC export of 560 mg m^{-2} d^{-1} (W. Bagniewski, submitted), and with an export estimate of 550 mg m^{-2} d^{-1} based on glider optical backscatter (Briggs et al., in prep.).

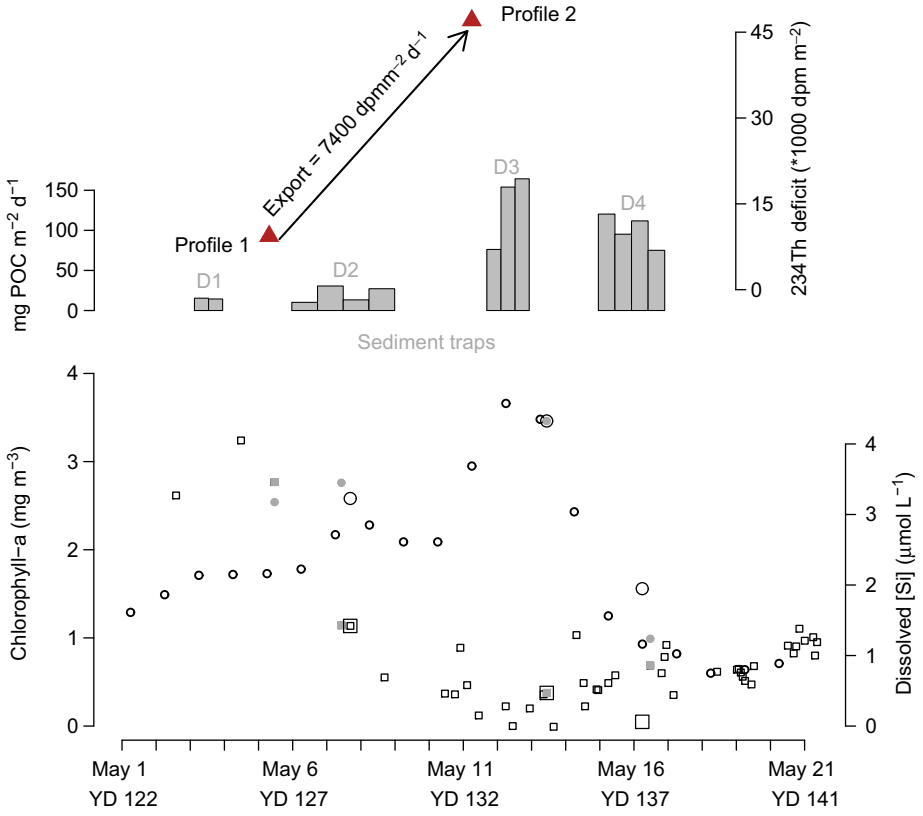

Fig. 8. Overview plot of the sediment trap and ^{234}Th results, together with daily mean chlorophyll-*a* concentration measured by the float (from fluorescence, small open circles) and mean silicate concentration in the upper 20 m inside the patch measured from bottle samples (small open squares). The local mean chlorophyll concentration in the upper 20 m where each trap deployment was made and each ^{234}Th profile taken is shown with closed grey circles (traps) and large open circles (^{234}Th). Similarly, the local mean silicate concentration in the upper 20 m for each trap deployment and ^{234}Th profile is shown with closed grey squares (traps) and large open squares (^{234}Th). For the trap POC fluxes, the total width of each group of bars indicates the collection period of that set of traps (i.e. 1 day for D1, 3 days for D2, etc.). The arrow between the ^{234}Th measurements indicates the growing depletion between Profile 1 and Profile 2, from which we diagnose a flux of 7400 dpm m^{-2} d^{-1}.

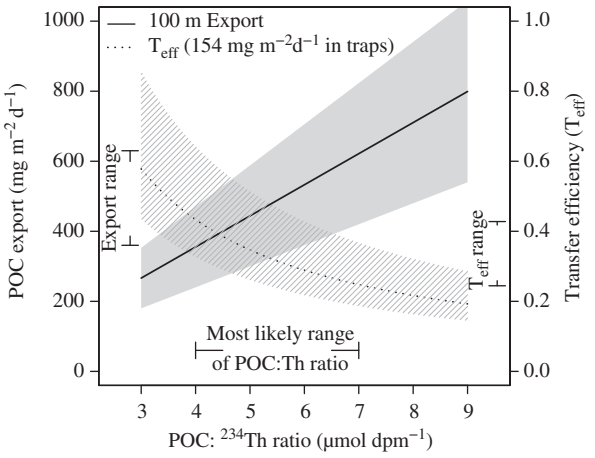

Fig. 9. Diagram showing the POC export at 100 m, calculated from ^{234}Th depletion, as a function of the POC:^{234}Th ratio. Also shown is the resulting transfer efficiency, T_{eff}, of the export at 100 m to the two deep traps on Deployment 3 (600 and 750 m), which caught nearly identical POC flux. T_{eff} is defined as the ratio of deep flux to shallow flux. We consider a likely range of POC:^{234}Th to be between 4 and 7 μmol POC dpm^{-1} (indicated on the *x*-axis), but as the large particle export event was not sampled at shallow depth, we are unable to constrain this ratio well. The resulting bounds on export and T_{eff} of a range in POC:^{234}Th ratio from 4 to 7 are marked on the corresponding *y*-axes.

4.3. Transfer efficiency

We can then estimate the transfer efficiency (defined as the percentage of the export flux that is collected at a particular depth) of the export event by comparing POC export at 100 m to the flux in the sediment traps. For this we use the mean POC flux of D3#600 and D3#750 (154 mg POC m^{-2} d^{-1}), which we believe to be most representative of the export event. Transfer efficiency is also plotted in Fig. 9, using the range of export values based on ^{234}Th. Given a POC:^{234}Th ratio between 4 and 7 μmol dpm^{-1}, the POC transfer efficiency ranges from 43 ± 11% to 25 ± 6%.

This transfer efficiency through the mesopelagic is high. In comparison, a Martin-type flux attenuation from 100 to 700 m, using $F_{700}=F_{100}(700/100)^{-0.86}$ (Martin et al., 1987) would give a transfer efficiency between 100 and 700 m of 19% (F_i=flux at depth *i* metres). The transfer efficiencies we obtained (25–43%) would correspond to a Martin-curve *b*-exponent between −0.71 and −0.43.

This calculation would be compromised if the traps had collected material derived partly from surface waters adjacent to the bloom patch. However, as those waters were mostly low in chlorophyll throughout our study (the region of high-chlorophyll water northeast of the patch was 40–60 km away), one would then expect the traps to collect less material than if they collected only particles from inside the patch, thus underestimating the true flux. In that case, the true transfer efficiency would be even higher than our estimate.

Our calculation further assumes that the traps collected with 100% efficiency. Although trapping efficiency can be calculated from the collected flux of natural radionuclides such as ^{234}Th (Buesseler et al., 2007), the depth difference between traps and calculated ^{234}Th export is too great in our case to do so reliably. We do note, however, that there was no major discrepancy in the ^{234}Th fluxes caught by the traps and the fluxes calculated from the ^{234}Th profiles. Hence we have no particular reason to question the trap results.

Our data are consistent with the comparison of regional studies by Buesseler and Boyd (2009), who found that a diatom bloom at 48°N in the Atlantic (Buesseler et al., 1992) had the highest transfer efficiency of the nine studies they examined (based on the data between 50 and 150 m, and a model down to 500 m). Our data thus confirm that diatom blooms can lead to large export and efficient transfer of POC through the mesopelagic.

4.4. Chemical composition of trap samples

The POC:PON ratios were notably low, mostly below the Redfield ratio of 6.6, and showed no clear increase with depth. This suggests that the particles were relatively undegraded, as carbon has a longer remineralization length-scale than nitrogen, and the POC:PON ratio is often above the Redfield ratio in sediment trap samples (Schneider et al., 2003).

The Si:POC ratios overall show a clear increase with depth, which could indicate POC remineralization (Nelson et al., 1996; Ragueneau et al., 2002). However, the low shallow values were all from D1 and D2, which caught a different particle pulse to the later traps. For instance, the D3 and D4 samples contained large numbers of broken diatom frustules, contributing mostly opal but little POC, but these were much less common in D1 and D2.

The high celestite fluxes, up to 100 mg m^{-2} d^{-1}, are not unexpected in this region. Acantharian cysts rarely sink below the first few 100 m, as their mineral shell dissolves (Antia et al., 1993; Bernstein et al., 1987; Michaels et al., 1995). In the Iceland Basin, however, Martin et al. (2010) found a particularly large and fast-sinking type of acantharian cyst (up to 1 mm long; sinking speed 500 m d^{-1}) in sediment traps at 2000 m during spring. The present study confirms that these cysts sink out annually during spring. Celestite is the densest oceanic biomineral (3.96 g cm^{-3}), hence one might speculate whether it ballasts a disproportionate amount of POC. However, the large, smooth-walled cysts in our samples were generally not entangled with aggregates. While celestite certainly increased the density of the cysts themselves (presumably leading to their high sinking speed), we consider it unlikely that celestite played a significant role in ballasting other particles. This could be investigated more thoroughly in future using sampling methods that preserve intact particles, such as polyacrylamide gels (Ebersbach and Trull, 2008).

The material caught during D3 and D4 was rich in TEP, and consisted primarily of phytodetritus. This is consistent with Passow et al. (2001), who found that diatom sedimentation was always associated with increased TEP sedimentation. It is also consistent with the hypothesis that TEP are required for particle aggregation during blooms (Alldredge and Jackson, 1995; Logan et al., 1995; Passow et al., 1994), as a large flux of phytodetritus should then be TEP-rich. Production of TEP may actually be an "overflow" mechanism for excess photosynthate produced by cells that are photosynthesising but unable to divide (Engel, 2000; Kahl et al., 2008), as would happen under silicate-limitation. It is therefore possible that the export event was triggered by silicate limitation, which increased TEP production that then led to particle aggregation and sinking.

5. Conclusions

We conclude that a sub-polar North Atlantic diatom bloom led to substantial export of particulate organic carbon in the form of phytoplankton aggregates during a sudden export event. These particles were rich in TEP, and had a high transfer efficiency through the mesopelagic. We hypothesise that sedimentation of the bloom occurred because silicate stress of diatoms lead to TEP production, which promoted aggregation and sinking.

Acknowledgements

Kevin Saw helped with PELAGRA deployments. Bob Head, Darryl Green, and Mark Stinchcombe helped with POC, PIC and

Sr, and BSi measurements, respectively. MODIS Aqua/Terra and MERIS data products were obtained from the National Aeronautical and Space Administration (NASA) OceanColor Web and European Space Agency MERCI Website. Brandon Sackmann processed the satellite data, with the support from NASA. Emily Kallin measured silicate, Paul Morris helped with analysing and interpreting the ^{234}Th measurements, and Sebastian Steigenberger provided advice on TEP measurement. We thank Tatiana Rynearson, Kirk Cochran, and two anonymous reviewers for helpful comments on the manuscript. This work is part of the lead author's doctoral research, and was funded by the UK Natural Environment Research Council and the US National Science Foundation.

Appendix A. Supporting information

Supplementary data associated with this article can be found in the online version at doi:10.1016/j.jdsr.2011.01.006.

References

Alldredge, A.L., Jackson, G.A., 1995. Aggregation in marine systems—preface. Deep-Sea Research Part II—Topical Studies in Oceanography 42 (1), 1–7.

Alldredge, A.L., Passow, U., Logan, B.E., 1993. The abundance and significance of a class of large, transparent organic particles in the ocean. Deep-Sea Research Part I—Oceanographic Research Papers 40 (6), 1131–1140.

Antia, A.N., Bauerfeind, E., von Bodungen, B., Zeller, U., 1993. Abundance, encystment and sedimentation of Acantharia during autumn 1990 in the East Greenland Sea. Journal of Plankton Research 15 (1), 99–114.

Armstrong, R.A., Lee, C., Hedges, J.I., Honjo, S., Wakeham, S.G., 2002. A new, mechanistic model for organic carbon fluxes in the ocean based on the quantitative association of POC with ballast minerals. Deep-Sea Research Part II—Topical Studies in Oceanography 49 (1–3), 219–236.

Beers, J.R., Stewart, G.L., 1970. The preservation of acantharians in fixed plankton samples. Limnology and Oceanography 15 (5), 825–827.

Bernstein, R.E., Betzer, P.R., Feely, R.A., Byrne, R.H., Lamb, M.F., Michaels, A.F., 1987. Acanthartian fluxes and strontium to chlorinity ratios in the North Pacific Ocean. Science 237 (4821), 1490–1494.

Buesseler, K.O., 1998. The decoupling of production and particulate export in the surface ocean. Global Biogeochemical Cycles 12 (2), 297–310.

Buesseler, K.O., Antia, A.N., Chen, M., Fowler, S.W., Gardner, W.D., Gustafsson, O., Harada, K., Michaels, A.F., van der Loeff, M.R., Sarin, M., Steinberg, D.K., Trull, T., 2007. An assessment of the use of sediment traps for estimating upper ocean particle fluxes. Journal of Marine Research 65 (3), 345–416.

Buesseler, K.O., Bacon, M.P., Cochran, J.K., Livingston, H.D., 1992. Carbon and nitrogen export during the JGOFS North Atlantic Bloom Experiment estimated from Th-234:U-238 disequilibria. Deep-Sea Research Part A—Oceanographic Research Papers 39 (7–8A), 1115–1137.

Buesseler, K.O., Benitez-Nelson, C.R., Moran, S.B., Burd, A., Charette, M., Cochran, J.K., Coppola, L., Fisher, N.S., Fowler, S.W., Gardner, W., Guo, L.D., Gustafsson, O., Lamborg, C., Masque, P., Miquel, J.C., Passow, U., Santschi, P.H., Savoye, N., Stewart, G., Trull, T., 2006. An assessment of particulate organic carbon to thorium-234 ratios in the ocean and their impact on the application of Th-234 as a POC flux proxy. Marine Chemistry 100 (3–4), 213–233.

Buesseler, K.O., Boyd, P.W., 2009. Shedding light on processes that control particle export and flux attenuation in the twilight zone of the open ocean. Limnology and Oceanography 54 (4), 1210–1232.

Bury, S.J., Boyd, P.W., Preston, T., Savidge, G., Owens, N.J.P., 2001. Size-fractionated primary production and nitrogen uptake during a North Atlantic phytoplankton bloom: implications for carbon export estimates. Deep-Sea Research Part I—Oceanographic Research Papers 48 (3), 689–720.

Chen, J.H., Edwards, R.L., Wasserburg, G.J., 1986. ^{238}U, ^{234}U and ^{232}Th in seawater. Earth and Planetary Science Letters 80, 241–251.

Dam, H.G., Drapeau, D.T., 1995. Coagulation efficiency, organic-matter glues and the dynamics of particles during a phytoplankton bloom in a mesocosm study. Deep-Sea Research Part II—Topical Studies in Oceanography 42 (1), 111–123.

Ebersbach, F., Trull, T.W., 2008. Sinking particle properties from polyacrylamide gels during the KErguelen Ocean and Plateau compared Study (KEOPS): zooplankton control of carbon export in an area of persistent natural iron inputs in the Southern Ocean. Limnology and Oceanography 53 (1), 212–224.

Engel, A., 2000. The role of transparent exopolymer particles (TEP) in the increase in apparent particle stickiness (alpha) during the decline of a diatom bloom. Journal of Plankton Research 22 (3), 485–497.

François, R., Honjo, S., Krishfield, R., Manganini, S., 2002. Factors controlling the flux of organic carbon to the bathypelagic zone of the ocean. Global Biogeochemical Cycles 16 (4). doi:10.1029/2001GB001722.

Gordon, L.I., Jennings, J.C., Ross, A.A., Krest, J.M., 1994. A suggested protocol for continuous flow automated analysis of seawater nutrients (phosphate, nitrate, nitrite and silicic acid) in the WOCE Hydrographic Program and the Joint Global Ocean Fluxes Study. WHP Operations and Methods. WOCE Hydrographic Program Office, Methods Manual 19-1.

Henson, S.A., Dunne, J.P., Sarmiento, J.L., 2009. Decadal variability in North Atlantic phytoplankton blooms. Journal of Geophysical Research—Oceans, 114. doi:10.1029/2008JC005139.

Henson, S.A., Sanders, R., Holeton, C., Allen, J.T., 2006. Timing of nutrient depletion, diatom dominance and a lower-boundary estimate of export production for Irminger Basin, North Atlantic. Marine Ecology-Progress Series 313, 73–84.

Honjo, S., Manganini, S.J., 1993. Annual biogenic particle fluxes to the interior of the North Atlantic Ocean studied at 34-Degrees-N 21-Degrees-W and 48-Degrees-N 21-Degrees-W. Deep-Sea Research Part II—Topical Studies in Oceanography 40 (1–2), 587–607.

Ingalls, A.E., Lee, C., Wakeham, S.G., Hedges, J.I., 2003. The role of biominerals in the sinking flux and preservation of amino acids in the Southern Ocean along 170 degrees W. Deep-Sea Research Part II—Topical Studies in Oceanography 50 (3–4), 713–738.

Kahl, L.A., Vardi, A., Schofield, O., 2008. Effects of phytoplankton physiology on export flux. Marine Ecology-Progress Series 354, 3–19.

Kiørboe, T., Hansen, J.L.S., Alldredge, A.L., Jackson, G.A., Passow, U., Dam, H.G., Drapeau, D.T., Waite, A., Garcia, C.M., 1996. Sedimentation of phytoplankton during a diatom bloom: rates and mechanisms. Journal of Marine Research 54 (6), 1123–1148.

Kiørboe, T., Tiselius, P., Mitchell-Innes, B., Hansen, J.L.S., Visser, A.W., Mari, X., 1998. Intensive aggregate formation with low vertical flux during an upwelling-induced diatom bloom. Limnology and Oceanography 43 (1), 104–116.

Klaas, C., Archer, D.E., 2002. Association of sinking organic matter with various types of mineral ballast in the deep sea: implications for the rain ratio. Global Biogeochemical Cycles 16 (4). doi:10.1029/2001GB001765.

Lampitt, R.S., 1985. Evidence for the seasonal deposition of detritus to the deep-sea floor and its subsequent resuspension. Deep-Sea Research Part A—Oceanographic Research Papers 32 (8), 885–897.

Lampitt, R.S., Boorman, B., Brown, L., Lucas, M., Salter, I., Sanders, R., Saw, K., Seeyave, S., Thomalla, S.J., Turnewitsch, R., 2008. Particle export from the euphotic zone: estimates using a novel drifting sediment trap, Th-234 and new production. Deep-Sea Research Part I—Oceanographic Research Papers 55 (11), 1484–1502.

Leblanc, K., Hare, C.E., Feng, Y., Berg, G.M., DiTullio, G.R., Neeley, A., Benner, I., Sprengel, C., Beck, A., Sanudo-Wilhelmy, S.A., Passow, U., Klinck, K., Rowe, J.M., Wilhelm, S.W., Brown, C.W., Hutchins, D.A., 2009. Distribution of calcifying and silicifying phytoplankton in relation to environmental and biogeochemical parameters during the late stages of the 2005 North East Atlantic Spring Bloom. Biogeosciences 6 (10), 2155–2179.

Lochte, K., Ducklow, H.W., Fasham, M.J.R., Stienen, C., 1993. Plankton succession and carbon cycling at 47-Degrees-N–20-Degrees-W during the JGOFS North Atlantic Bloom Experiment. Deep-Sea Research Part II—Topical Studies in Oceanography 40 (1–2), 91–114.

Logan, B.E., Passow, U., Alldredge, A.L., Grossart, H.P., Simon, M., 1995. Rapid formation and sedimentation of large aggregates is predictable from coagulation rates (half-lives) of transparent exopolymer particles (TEP). Deep-Sea Research Part II—Topical Studies in Oceanography 42 (1), 203–214.

Maiti, K., Benitez-Nelson, C.R., Buesseler, K.O., 2010. Insights into particle formation and remineralization using the short-lived radionuclide, Thorium-234. Geophysical Research Letters, 37. doi:10.1029/2010GL044063.

Martin, J.H., Knauer, G.A., Karl, D.M., Broenkow, W.W., 1987. VERTEX—carbon cycling in the Northeast Pacific. Deep-Sea Research Part A—Oceanographic Research Papers 34 (2), 267–285.

Martin, P., Allen, J.T., Cooper, M.J., Johns, D.G., Lampitt, R.S., Sanders, R., Teagle, D.A.H., 2010. Sedimentation of acantharian cysts in the Iceland Basin: strontium as a ballast for deep ocean particle flux, and implications for acantharian reproductive strategies. Limnology and Oceanography 55 (2), 604–614.

Michaels, A.F., Caron, D.A., Swanberg, N.R., Howse, F.A., Michaels, C.M., 1995. Planktonic sarcodines (Acantharia, Radiolaria, Foraminifera) in surface waters near Bermuda—abundance, biomass and vertical flux. Journal of Plankton Research 17 (1), 131–163.

Mortlock, R.A., Froelich, P.N., 1989. A simple method for the rapid determination of biogenic opal in pelagic marine sediments. Deep-Sea Research Part A—Oceanographic Research Papers 36 (9), 1415–1426.

Murray, J.W., Young, J., Newton, J., Dunne, J., Chapin, T., Paul, B., McCarthy, J.J., 1996. Export flux of particulate organic carbon from the central equatorial Pacific determined using a combined drifting trap Th-234 approach. Deep-Sea Research Part II—Topical Studies in Oceanography 43 (4–6), 1095–1132.

Nelson, D.M., DeMaster, D.J., Dunbar, R.B., Smith, W.O., 1996. Cycling of organic carbon and biogenic silica in the Southern Ocean: estimates of water-column and sedimentary fluxes on the Ross Sea continental shelf. Journal of Geophysical Research—Oceans 101 (C8), 18519–18532.

Passow, U., 2002. Transparent exopolymer particles (TEP) in aquatic environments. Progress in Oceanography 55 (3–4), 287–333.

Passow, U., Alldredge, A.L., 1995a. A dye-binding assay for the spectrophotometric measurement of transparent exopolymer particles (TEP). Limnology and Oceanography 40 (7), 1326–1335.

Passow, U., Alldredge, A.L., 1995b. Aggregation of a diatom bloom in a mesocosm—the role of transparent exopolymer particles (TEP). Deep-Sea Research Part II—Topical Studies in Oceanography 42 (1), 99–109.

Passow, U., Alldredge, A.L., Logan, B.E., 1994. The role of particulate carbohydrate exudates in the flocculation of diatom blooms. Deep-Sea Research Part I—Oceanographic Research Papers 41 (2), 335–357.

Passow, U., Dunne, J., Murray, J.W., Balistrieri, L., Alldredge, A.L., 2006. Organic carbon to Th-234 ratios of marine organic matter. Marine Chemistry 100 (3–4), 323–336.

Passow, U., Shipe, R.F., Murray, A., Pak, D.K., Brzezinski, M.A., Alldredge, A.L., 2001. The origin of transparent exopolymer particles (TEP) and their role in the sedimentation of particulate matter. Continental Shelf Research 21 (4), 327–346.

Ragueneau, O., Dittert, N., Pondaven, P., Treguer, P., Corrin, L., 2002. Si/C decoupling in the world ocean: is the Southern Ocean different? Deep-Sea Research Part II—Topical Studies in Oceanography 49 (16), 3127–3154.

Ragueneau, O., Schultes, S., Bidle, K., Claquin, P., La Moriceau, B., 2006. Si and C interactions in the world ocean: importance of ecological processes and implications for the role of diatoms in the biological pump. Global Biogeochemical Cycles 20 (4). doi:10.1029/2006GB002688.

Reigstad, M., Wassmann, P., 2007. Does *Phaeocystis* spp. contribute significantly to vertical export of organic carbon? Biogeochemistry 83 (1–3), 217–234.

Rutgers van der Loeff, M.M., Moore, W.S., 1999. Determination of natural radioactive tracers. In: Grasshoff, K., Ehrhardt, M., Kremling, K. (Eds.), Methods of Seawater Analysis. Verlag Chemie, Weinheim, pp. 365–397.

Salter, I., Lampitt, R.S., Sanders, R., Poulton, A., Kemp, A.E.S., Boorman, B., Saw, K., Pearce, R., 2007. Estimating carbon, silica and diatom export from a naturally fertilised phytoplankton bloom in the Southern Ocean using PELAGRA: a novel drifting sediment trap. Deep-Sea Research Part II—Topical Studies in Oceanography 54 (18–20), 2233–2259.

Savidge, G., Boyd, P., Pomroy, A., Harbour, D., Joint, I., 1995. Phytoplankton production and biomass estimates in the Northeast Atlantic Ocean, May to June 1990. Deep-Sea Research Part I—Oceanographic Research Papers 42 (5), 599–617.

Savoye, N., Benitez-Nelson, C., Burd, A.B., Cochran, J.K., Charette, M., Buesseler, K.O., Jackson, G.A., Roy-Barman, M., Schmidt, S., Elskens, M., 2006. Th-234 sorption and export models in the water column: a review. Marine Chemistry 100 (3–4), 234–249.

Schneider, B., Schlitzer, R., Fischer, G., Nothig, E.M., 2003. Depth-dependent elemental compositions of particulate organic matter (POM) in the ocean. Global Biogeochemical Cycles 17 (2). doi:10.1029/2002GB001871.

Siegel, D.A., Fields, E., Buesseler, K.O., 2008. A bottom-up view of the biological pump: modelling source funnels above ocean sediment traps. Deep-Sea Research Part I—Oceanographic Research Papers 55, 108–127.

Sieracki, M.E., Verity, P.G., Stoecker, D.K., 1993. Plankton community response to sequential silicate and nitrate depletion during the 1989 North Atlantic Spring Bloom. Deep-Sea Research Part II—Topical Studies in Oceanography 40 (1–2), 213–225.

Turner, J.T., 2002. Zooplankton fecal pellets, marine snow and sinking phytoplankton blooms. Aquatic Microbial Ecology 27, 57–105.

Thomalla, S., Turnewitsch, R., Lucas, M., Poulton, A., 2006. Particulate organic carbon export from the North and South Atlantic gyres: the Th-234/U-238 disequilibrium approach. Deep-Sea Research Part II—Topical Studies in Oceanography 53 (14–16), 1629–1648.